Electrical pumping and tuning of exciton-polaritons in carbon nanotube microcavities

Arko Graf[1,2†], Martin Held[1†], Yuriy Zakharko[1], Laura Tropf[2], Malte C. Gather[2]*, and Jana Zaumseil[1]*

[1] *Institute for Physical Chemistry, Universität Heidelberg, D-69120 Heidelberg, Germany*

[2] *Organic Semiconductor Centre, SUPA, School of Physics and Astronomy, University of St Andrews, St Andrews KY16 9SS, United Kingdom*

[†]These authors contributed equally to this work.

* E-mail: mcg6@st-andrews.ac.uk, zaumseil@uni-heidelberg.de

Abstract

Exciton-polaritons are hybrid light-matter particles that form upon strong coupling of an excitonic transition to a cavity mode. As bosons, polaritons can form condensates with coherent laser-like emission. For organic materials optically pumped condensation was achieved at room-temperature but electrically pumped condensation remains elusive due to insufficient polariton densities. Here we combine the outstanding optical and electronic properties of purified, solution-processed semiconducting (6,5) single-walled carbon nanotubes (SWCNTs) in a microcavity-integrated light-emitting field-effect transistor to realize efficient electrical pumping of exciton-polaritons at room temperature with high current densities (>10 kA cm^{-2}) and tunability in the near-infrared (1060 nm to 1530 nm). We demonstrate thermalization of SWCNT polaritons, exciton-polariton pumping rates ~10^4 times higher than in current organic polariton devices, direct control over the coupling strength (Rabi splitting) via the applied gate voltage and a tenfold enhancement of polaritonic over excitonic emission. This powerful material-device combination paves the way to carbon-based polariton emitters and possibly lasers.

Exciton-polaritons are hybrid light-matter quasiparticles with mixed photonic (small effective mass) and excitonic (strong nonlinearities and fast relaxation) properties that enable a rich set of quantum phenomena as well as optoelectronic applications.[1–4] One of them is the polariton laser, in which stimulated scattering of the bosonic polaritons leads to a macroscopic condensate and to coherent laser-like emission at thresholds orders of magnitude below conventional photon lasing.[1,5,6] Organic semiconductors have recently attracted much attention in this area because the nature of their excitonic transitions results in particularly strong light-matter coupling and facilitates polariton lasing at room temperature.[7–10] However, electrically pumped exciton-polariton devices based on organic semiconductors have not yet reached the current densities required for polariton condensation, mainly due to the low charge carrier mobilities in these materials.[3]

Previous work on electrically pumped exciton-polaritons either employed multilayer light-emitting diodes (LED), in which the direction of current flow and optical feedback coincided,[5,11,12] or achieved optical feedback orthogonal to the optical feedback by using complex semiconductor fabrication technology.[6] By comparison, light-emitting field-effect transistors (LEFETs) can be produced by relatively simple techniques while enabling very high current densities that are unaffected by the presence of an optical feedback structure due to the in-plane current flow.[13] An ideal emitter material will support and withstand high current densities and retain a high oscillator strength under such conditions. Although charge accumulation and the resulting reduction in oscillator strength have been used to tune the position of polariton branches,[14] these effects may ultimately lead to a loss of light-matter hybridization at the high current densities required for condensation.[15] To avoid this, materials with high charge carrier mobility are necessary. In addition, any potential material must provide channels for fast polariton relaxation under electrical pumping in order to achieve rapid accumulation of polaritons in the ground state, ideally at room

temperature. Meeting all these requirements simultaneously has proven very challenging – some of the required material properties are inherent to organic emitters, while others are typically observed only in inorganic semiconductors.[3,16,17] Hence, there is an urgent need for a material and a matching device geometry that combine these criteria.

We recently reported strong coupling and optically pumped exciton-polaritons in the near-infrared at room-temperature using metal-clad microcavities filled with semiconducting single-walled carbon nanotubes (SWCNTs) embedded in a polymer matrix.[18] Even at moderate concentrations of SWCNTs (~2 wt%), we found a Rabi splitting of more than 120 meV, which we attributed to the high oscillator strength of SWCNTs. Carbon nanotubes can be readily processed from solution, exhibit exceptionally high electron and hole mobilities even in random networks[19] and show electroluminescence in the near infrared.[20] In addition, exciton relaxation in SWCNTs is extremely fast (~ 40 fs) due to strong exciton-phonon interactions[21], which may be helpful to achieve polariton condensation. The unique one-dimensionality of the excitons and the low energetic disorder in monochiral SWCNT samples further support efficient relaxation via exciton-exciton scattering[22] and strong non-linearities.[23]

Here, we demonstrate electrically pumped near-infrared exciton-polariton emission at room temperature using a SWCNT-based ambipolar LEFET that is embedded in an optical microcavity. The resulting strong coupling leads to a Rabi splitting of ~48 meV, with electrically pumped polariton emission and efficient polariton relaxation even at very high current densities. Simple adjustments in cavity thickness facilitate tuning of the narrow-band polariton electroluminescence (EL) from 1060 nm up to 1530 nm. Furthermore, we reversibly modify the coupling strength in LEFETs by unipolar charge carrier accumulation. SWCNT-based LEFETs are thus an ideal platform to investigate the fundamental properties of exciton-polaritons and in the future may enable electrically pumped, carbon-based polariton lasers.

Cavity-integrated light-emitting SWCNT transistors

We used (6,5) SWCNTs that were dispersed and sorted by selective polymer-wrapping using high-speed shear force mixing[24] (see Methods). Dense, spin-coated films (Supplementary Fig. S1) exhibited a narrow absorption peak at 1.246 eV (995 nm, excitonic S_1 transition) and a photoluminescence (PL) peak at 1.234 eV (1005 nm, Figure 1a) with a PL quantum yield (PLQY) of 0.17 %. The PL sideband located about 140 meV below the S_1-exciton is related to phonon-assisted brightening of dark excitons.[25] We integrated these dense SWCNT films into bottom-contact/top-gate LEFETs (see Methods). No additional charge injection layers are needed in LEFETs and thus the excellent electronic properties of the SWCNTs are fully exploited. The optical cavity was formed perpendicular to the direction of charge transport by the silver gate electrode and a semitransparent bottom mirror (Figure 1b). The bottom mirror was electrically separated from the LEFET by an aluminum oxide spacer layer that also allowed us to adjust the cavity thickness and thus the spectral position of the cavity mode without affecting charge transport in the LEFET (Supplementary Section 1, Table S1). The LEFETs were operated at room temperature and under ambient conditions.

Our LEFETs showed ambipolar charge transport (Figure 1c) with high on/off current ratios of up to 10^6 at low drain bias (V_d = -0.5 V). The high electron and hole mobilities of 4.2 and 3.5 $cm^2\ V^{-1}\ s^{-1}$, respectively, enabled us to operate the LEFET continuously at high current densities (>10 kA/cm^2). We also fabricated a reference LEFET without a bottom mirror to examine the influence of the cavity on charge transport and injection but did not observe any significant differences in the electrical performance (Supplementary Figs. S2 and S3).[26]

In the ambipolar regime of LEFETs (V_d = −8 V) electrons and holes are injected into the channel simultaneously and meet within a narrow zone to form excitons that can decay radiatively. Consequently, the charge carrier density reaches a minimum in this recombination zone.[27] The

position of the emission zone (observed width ~1 μm) within the channel can be adjusted by the applied gate voltage V_g (Figure 1d and supplementary video).

Electrically pumped exciton-polaritons

In order to investigate light-matter coupling and polariton emission in these LEFETs, we performed angle-resolved spectroscopy using Fourier imaging. Figure 2a shows the angle-dependent reflectivity of the LEFET cavity within the channel for TE polarization (see Supplementary Fig. S4 for TM). Clear anticrossing of the exciton (X) and cavity mode (CM) is observed and an upper (UP) and lower polariton (LP) branch are present. From these data we extract a Rabi splitting of 125 meV. This value is in good agreement with a fit of the observed modes to the coupled oscillator model (dashed lines in Fig. 2a; Rabi splitting, $\hbar\Omega$ = 127 meV; cavity-detuning, $\Delta = -62$ meV) assuming an effective refractive index $n_{\text{eff}}^{\text{TE}}$ of 1.96 (extracted from a cavity without nanotubes, Supplementary Fig. S5). Taking into account the measured cavity and exciton damping rates as defined by their linewidth, light-matter hybridization is achieved in these cavity-embedded LEFETs for a Rabi splitting larger than 23 meV (see Methods), thus placing our cavities firmly in the strong coupling regime. Upon optical excitation of the SWCNTs, we observed polariton emission along the lower polariton branch (Figure 2b). These results are in agreement with our previous report on SWCNT polaritons.[18] However, the cavity-integrated LEFETs also exhibited electroluminescence (EL) from the LP branch and thus electrically pumped polariton emission. Figure 2c shows the angle-resolved EL spectrum at a current density (J_{ds}) of 600 A cm^{-2}, revealing a steep increase in emission intensity toward smaller angles (50 % of the light is emitted within a 20° cone). The fractions of photonic and excitonic character of the polaritons were calculated with a coupled oscillator model (Figure 2d) revealing a significant excitonic fraction

(> 25%), even at k = 0, which will promote fast excitonic relaxation of polaritons. Knowing the light-matter hybridization level allows us to calculate the polariton occupancy along the LP branch (Supplementary Fig. S6). We find the LP occupation to be thermalized which confirms that there is indeed efficient relaxation of the electrically pumped polaritons towards k = 0. We did not observe any angular linewidth broadening of the EL compared to the PL signal. A significant influence of emission from a confined zone (1 µm orthogonal to the electrodes, emitting into a range of angles ~9°) can thus be excluded.

Emission efficiency and wavelength tuning

To further evaluate the relaxation and emission efficiency of our devices, we measured the external quantum efficiency (see Methods) of a cavity-embedded LEFET compared to a reference without a bottom mirror (Figure 3a). For the first generation of cavity-embedded LEFETs (SWCNT film thickness 33 nm), the EQE was approximately sevenfold lower than the reference device. We partially attribute this reduction in EQE to the substantial surface roughness of the SWCNT films (Supplementary Fig. S1a), which reduces the cavity quality and thus disturbs the build-up of the electric field inside the cavity. Additional losses are attributed to the exciton-to-polariton conversion efficiency that result from non-optimal detuning (see below). However, despite the lower absolute value, the cavity-device showed no substantial EQE roll-off even at current densities above 1,000 A cm^{-2}, which suggests that quenching effects, such as exciton-exciton annihilation, do not prevent dense accumulation of polaritons.

To improve the optical quality of our cavities and thus increase the EQE, we fabricated cavity-embedded LEFETs with a thinner (19 nm) and smoother SWCNT film (Supplementary Fig. S1b). The angle and spectrally resolved reflectivity of these LEFETs showed a Rabi splitting of 48 meV (Figure 3b). The angle-resolved EL again followed the LP branch and showed efficient

relaxation towards k = 0 (Figure 3c, Supplementary Fig. S6). This LEFET also showed a drastically higher EQE (Figure 3a). We attribute this increase to a higher PL quantum yield of the smoother SWCNT film (0.28 %) and to the improved optical quality of the cavity, which led to longer polariton lifetimes as indicated by the narrower linewidth of the LP (half width at half maximum (HWHM) of 16 meV compared to 27 meV). In addition, the difference in detuning and coupling strength leads to a higher photon character of the LP at k = 0.

By adjusting the thickness of the oxide spacer layer and thus the cavity resonance, we could readily tune the polariton emission across a wide spectral range. Using LEFETs with identical monochiral films of (6,5) nanotubes (thickness 19 nm), we obtained narrow-band EL spectra (FWHM < 35 nm) with peak emission ranging from 1060 nm to 1530 nm. Figure 3d shows the EL spectra (normal to the sample surface) for several representative detuning values Δ (see Supplementary Fig. S7 for angular spectra). The EQE of these devices depended strongly on the energetic separation between the exciton and LP at k = 0 (Figure 3e). Since all devices exhibited nearly identical electrical performance (Supplementary Fig. S3), this is attributed to different efficiencies of scattering from the exciton reservoir into the LP branch. Non-radiative and radiative channels have been discussed as possible pumping mechanisms of the LP branch, with the dominant mechanism depending strongly on the material.[28,29] In our case the decrease in EQE for a detuning larger than 200 meV suggests that radiative pumping, similar to Förster energy transfer, of the LP is not the dominant scattering process.[28] Instead, we observed the highest overall EQE when the LP was 60 - 160 meV below the exciton energy. While this range overlaps with the phonon-assisted excitonic emission[25] of bare (6,5) SWCNTs (see PL spectra, Fig. 1a), radiative pumping from this vibrational sideband is unlikely due to its small intensity compared to the main exciton emission. Instead, direct population of the LP branch from the exciton reservoir via phonon emission may lead to efficient scattering similar to other organic materials.[30,31] The pronounced

population of the LP branch at 165 meV below the exciton energy (Supplementary Fig. S7e) is consistent with a population that is assisted by a D-phonon (~160 meV).[25] For electrical pumping, polariton-electron scattering is another potential relaxation path as discussed for inorganic materials.[32]

Polariton relaxation and high current densities

Further insight into the involved processes was gained by comparing a cavity-embedded LEFET with a 170 nm spacer layer and a dense SWCNT film (thickness, 19 nm) to a microcavity with a ~250 nm-thick low density SWCNT layer (insets Figure 4a). The thickness of the second cavity was adjusted to yield the same Rabi splitting and cavity detuning as the LEFET cavity (see Supplementary Fig. S8)[18]. While both SWCNT layers showed similar effective oscillator strength and polariton dispersion, a direct comparison of the angle-resolved PL spectra revealed a crucial difference: the cavity-embedded LEFET with the dense SWCNT layer did not exhibit a bottleneck for polariton relaxation whereas –for the same excitation conditions– the low SWCNT concentration cavity did (Figure 4a). We attribute the enhanced relaxation rate to the higher SWCNT density, which supports non-radiative intertube relaxation[33] in addition to any radiative pumping of the LP from the exciton reservoir.[7,34] The former process is closely related to intermolecular energy transfer and thus depends on intertube distance.

As outlined above, achieving high current densities while maintaining strong coupling is a critical requirement for electrically pumped polariton lasing. The spectral characteristics of the polariton emission from our cavity-embedded LEFETs remained largely unchanged over a very wide current density range from 128 A cm^{-2} up to 18,600 A cm^{-2} (Figure 4b). Although continuous operation at such high current densities may lead to Joule heating of the channel region,[36] which

may affect polariton relaxation, we did not observe any measurable degradation. We attribute this remarkable device stability to the high thermal conductivity of SWCNTs (~3000 W $m^{-1}K^{-1}$),[37] their high carrier mobilities and excellent photostability. Even for the maximum current density tested here, strong coupling was retained and Rabi splitting (determined from reflectivity measurements, Figure 4c) reduced only slightly – presumably due to transient ground state bleaching. We attribute this to the high charge carrier mobilities in the dense SWCNT network, the limited thickness (few nm) of the charge accumulation layer and the ambipolar operation of the LEFET, which minimizes the charge carrier concentration within the recombination and emission zone[27].

Since in ambipolar LEFETs all injected charges form excitons, we can readily estimate the exciton pumping rate (Supplementary Section 2) and obtain a value of ~10^{27} cm^{-3} s^{-1}, which is ~10^4 times higher than the values previously reported for electrical pumping of exciton-polaritons in organic light-emitting diodes (OLED).[11,12,35] We reach a polariton density of ~$3.6 \cdot 10^{11}$ cm^{-3}, which is well below the Mott transition (see Supplementary Section 2 and 3) and possible exciton-exciton interaction based on exciton diffusion. Hence we do not observe nonlinear interactions in our devices. In an improved microcavity-LEFET (see below) polariton densities of 10^{14} cm^{-3} are readily achievable. In this regime, nonlinear interactions might be present for hybrid exciton-polaritons.

Tuning the Rabi-splitting via applied voltage

So far we operated our LEFETs in the ambipolar regime to achieve charge recombination and emission at high current densities. However, the LEFET geometry also allows us to accumulate a defined density of charge carriers by operating them in the unipolar regime at low drain voltages. When applying a gate voltage and thus charging a portion of SWCNTs in the cavity, their ground

state is bleached and thus the overall oscillator strength of the strongly coupled S_1 transition is reduced.[38,39] This allows us to reversibly change the coupling from strong to weak (Figure 5a) and thus tune the polariton dispersion. With increasing negative gate voltage and thus hole density in the channel, the coupling strength decreased and at around −10.6 V no splitting of the UP and LP branches was detected anymore – a condition associated with the weak coupling regime (Figure 5b). The square of the Rabi splitting reduced linearly with gate voltage for $V_g \lesssim$ -5V, consistent with the expectation that below a threshold voltage the hole density scales linearly with gate voltage and that Rabi splitting scales with the square-root of the number of coupled oscillators.[40] The original coupling strength was recovered after the gate voltage was turned off. We were thus able to reversibly switch between strong and weak coupling and to modulate the Rabi splitting by more than 15 meV.

This effect could be used to precisely adjust the energetic position of the LP branch. We observed a shift of the LP emission at k = 0 of up to 7 meV in the PL spectra of these gated cavities (Supplementary Fig. S9). Further, the emission from the uncharged SWCNT layer showed more efficient relaxation towards the bottom of the LP branch than the charged film with lower coupling strength, which we attribute to the higher excitonic character of the LP in the former case. While excitonic absorption and emission efficiency are reduced upon charge accumulation, the addition of holes or electrons to SWCNTs also leads to red-shifted trion absorption and emission.[38] Interestingly, this could result in the formation of charged polaritons, which have previously been investigated in inorganic[41,42] and layered materials[43] and for which intriguing phenomena, e.g. room-temperature superconductivity[44] and enhanced relaxation[45], were predicted. Hence, cavity-embedded LEFETs represent a powerful tool to electrically tune fundamental properties of polaritons and facilitate investigation of additional hybridized states, such as, trion-polaritons.

Conclusion and Outlook

We have demonstrated efficient electrical pumping of near-infrared exciton-polaritons at room temperature using strongly coupled LEFET-cavities based on (6,5) SWCNT films. SWCNTs exhibit superior charge-transport properties compared to other solution-processed organic semiconductors,[46] while at the same time offering large oscillator strength. The LEFET geometry with its in-plane charge injection is particularly well-suited to exploit the high carrier mobilities in SWCNT networks. This combination of device geometry and material allowed us to maintain strong coupling in cavity-embedded LEFETs – even at very high current densities (>10 kA cm^{-2}). The electrically driven polariton emission is directional, features narrow linewidths and can be tuned from 1060 to 1530 nm by simply changing the cavity detuning rather than the emitter. This should make tedious purification of SWCNTs with different chiralities for different emission wavelengths obsolete and could open opportunities for applications in the telecom wavelengths window. Moreover, the coupling strength of the cavities was tuned by changing the carrier concentration via the applied gate voltage, which could also enable the investigation of trion-polaritons.

An estimation of the polariton density in cavity-embedded LEFETs with (6,5) SWCNTs (~$3.6 \cdot 10^{11}$ cm^{-3}) and ground state occupancy (0.004, Supplementary Section 2) suggests that reaching an occupancy larger than unity at k = 0 and thus the polariton lasing threshold is within realistic reach with optimized cavities and device fabrication (Supplementary Section 3). Hence, cavity-embedded LEFETs based on SWCNTs are a promising material/device combination that may ultimately lead to electrically pumped polariton lasing in carbon-based semiconductors at room temperature.

References

1. Kasprzak, J. *et al.* Bose–Einstein condensation of exciton polaritons. *Nature* **443,** 409–414 (2006).

2. Amo, A. *et al.* Superfluidity of polaritons in semiconductor microcavities. *Nat. Phys.* **5,** 805–810 (2009).

3. Sanvitto, D. & Kéna-Cohen, S. The road towards polaritonic devices. *Nat. Mater.* **15,** 1061–1073 (2016).

4. Dreismann, A. *et al.* A sub-femtojoule electrical spin-switch based on optically trapped polariton condensates. *Nat. Mater.* **15,** 1074–1078 (2016).

5. Schneider, C. *et al.* An electrically pumped polariton laser. *Nature* **497,** 348–352 (2013).

6. Bhattacharya, P. *et al.* Room Temperature Electrically Injected Polariton Laser. *Phys. Rev. Lett.* **112,** 236802 (2014).

7. Kéna-Cohen, S. & Forrest, S. R. Room-temperature polariton lasing in an organic single-crystal microcavity. *Nat. Photonics* **4,** 371–375 (2010).

8. Plumhof, J. D., Stöferle, T., Mai, L., Scherf, U. & Mahrt, R. F. Room-temperature Bose–Einstein condensation of cavity exciton–polaritons in a polymer. *Nat. Mater.* **13,** 247–252 (2013).

9. Daskalakis, K. S., Maier, S. A., Murray, R. & Kéna-Cohen, S. Nonlinear interactions in an organic polariton condensate. *Nat. Mater.* **13,** 271–8 (2014).

10. Dietrich, C. P. *et al.* An exciton-polariton laser based on biologically produced fluorescent protein. *Sci. Adv.* **2,** e1600666–e1600666 (2016).

11. Gubbin, C. R., Maier, S. A. & Kéna-Cohen, S. Low-voltage polariton electroluminescence from an ultrastrongly coupled organic light-emitting diode. *Appl. Phys. Lett.* **104,** 233302 (2014).

12. Christogiannis, N. *et al.* Characterizing the Electroluminescence Emission from a Strongly Coupled Organic Semiconductor Microcavity LED. *Adv. Opt. Mater.* **1,** 503–509 (2013).

13. Bisri, S. Z., Takenobu, T. & Iwasa, Y. The pursuit of electrically-driven organic semiconductor lasers. *J. Mater. Chem. C* **2,** 2827-2836 (2014).

14. Tsotsis, P. *et al.* Tuning the Energy of a Polariton Condensate via Bias-Controlled Rabi Splitting. *Phys. Rev. Appl.* **2,** 014002 (2014).

15. Tsintzos, S. I., Pelekanos, N. T., Konstantinidis, G., Hatzopoulos, Z. & Savvidis, P. G. A GaAs polariton light-emitting diode operating near room temperature. *Nature* **453,** 372–375 (2008).

16. Shiny condensates. *Nat. Mater.* **15,** 1047–1047 (2016).

17. Fraser, M. D., Höfling, S. & Yamamoto, Y. Physics and applications of exciton–polariton lasers. *Nat. Mater.* **15,** 1049–1052 (2016).

18. Graf, A., Tropf, L., Zakharko, Y., Zaumseil, J. & Gather, M. C. Near-infrared exciton-polaritons in strongly coupled single-walled carbon nanotube microcavities. *Nat. Commun.* **7,** 13078 (2016).

19. Schießl, S. P. *et al.* Polymer-sorted semiconducting carbon nanotube networks for high-performance ambipolar field-effect transistors. *ACS Appl. Mater. Interfaces* **7,** 682–9 (2015).

20. Khasminskaya, S. *et al.* Fully integrated quantum photonic circuit with an electrically driven light source. *Nat. Photonics* **10,** 727–732 (2016).

21. Soavi, G., Scotognella, F., Lanzani, G. & Cerullo, G. Ultrafast Photophysics of Single-Walled Carbon Nanotubes. *Adv. Opt. Mater.* **11**, 1670-1688 (2016).

22. Nguyen, D. T. *et al.* Elastic Exciton-Exciton Scattering in Photoexcited Carbon Nanotubes. *Phys. Rev. Lett.* **107,** 127401 (2011).

23. Iwamura, M. *et al.* Nonlinear Photoluminescence Spectroscopy of Carbon Nanotubes with Localized Exciton States. *ACS Nano* **8,** 11254–11260 (2014).

24. Graf, A. *et al.* Large scale, selective dispersion of long single-walled carbon nanotubes with high photoluminescence quantum yield by shear force mixing. *Carbon* **105,** 593–599 (2016).

25. Blackburn, J. L., Holt, J. M., Irurzun, V. M., Resasco, D. E. & Rumbles, G. Confirmation of K-Momentum Dark Exciton Vibronic Sidebands Using 13 C-labeled, Highly Enriched (6,5) Single-walled Carbon Nanotubes. *Nano Lett.* **12,** 1398–1403 (2012).

26. Orgiu, E. *et al.* Conductivity in organic semiconductors hybridized with the vacuum field. *Nat. Mater.* **14,** 1123–1129 (2015).

27. Gwinner, M. C. *et al.* Highly Efficient Single-Layer Polymer Ambipolar Light-Emitting Field-Effect Transistors. *Adv. Mater.* **24,** 2728–2734 (2012).

28. Grant, R. T. *et al.* Efficient Radiative Pumping of Polaritons in a Strongly Coupled Microcavity by a Fluorescent Molecular Dye. *Adv. Opt. Mater.* **4,** 1615–1623 (2016).

29. Ballarini, D. *et al.* Polariton-Induced Enhanced Emission from an Organic Dye under the Strong Coupling Regime. *Adv. Opt. Mater.* **2,** 1076–1081 (2014).

30. Coles, D. M. *et al.* Vibrationally Assisted Polariton-Relaxation Processes in Strongly Coupled Organic-Semiconductor Microcavities. *Adv. Funct. Mater.* **21,** 3691–3696 (2011).

31. Somaschi, N. *et al.* Phonon-driven resonantly enhanced polariton luminescence in organic

microcavities. in *Proc. SPIE* **8260,** 82600Q (2012).

32. Lagoudakis, P. G. *et al.* Electron-Polariton Scattering in Semiconductor Microcavities. *Phys. Rev. Lett.* **90,** 206401 (2003).

33. Rother, M., Schießl, S. P., Zakharko, Y., Gannott, F. & Zaumseil, J. Understanding Charge Transport in Mixed Networks of Semiconducting Carbon Nanotubes. *ACS Appl. Mater. Interfaces* **8,** 5571–5579 (2016).

34. Coles, D. M. *et al.* Polariton-mediated energy transfer between organic dyes in a strongly coupled optical microcavity. *Nat. Mater.* **13,** 712–719 (2014).

35. Tischler, J. R., Bradley, M. S., Bulović, V., Song, J. H. & Nurmikko, A. Strong Coupling in a Microcavity LED. *Phys. Rev. Lett.* **95,** 036401 (2005).

36. Nikiforov, G. O. *et al.* Current-Induced Joule Heating and Electrical Field Effects in Low Temperature Measurements on TIPS Pentacene Thin Film Transistors. *Adv. Electron. Mater.* **2,** 1600163 (2016).

37. Balandin, A. A. Thermal properties of graphene and nanostructured carbon materials. *Nat. Mater.* **10,** 569–581 (2011).

38. Jakubka, F., Grimm, S. B., Zakharko, Y., Gannott, F. & Zaumseil, J. Trion Electroluminescence from Semiconducting Carbon Nanotubes. *ACS Nano* **8,** 8477–8486 (2014).

39. Hartleb, H., Späth, F. & Hertel, T. Evidence for Strong Electronic Correlations in the Spectra of Gate-Doped Single-Wall Carbon Nanotubes. *ACS Nano* **9,** 10461–10470 (2015).

40. Lidzey, D. G. *et al.* Strong exciton-photon coupling in an organic semiconductor microcavity. *Nature* **395,** 53–55 (1998).

41. Rapaport, R. *et al.* Negatively Charged Quantum Well Polaritons in a GaAs/AlAs Microcavity: An Analog of Atoms in a Cavity. *Phys. Rev. Lett.* **84,** 1607–1610 (2000).

42. Rapaport, R., Cohen, E., Ron, A., Linder, E. & Pfeiffer, L. N. Negatively charged polaritons in a semiconductor microcavity. *Phys. Rev. B* **63,** 235310 (2001).

43. Sidler, M. *et al.* Fermi polaron-polaritons in charge-tunable atomically thin semiconductors. *Nat. Phys.* **1,** 255-261 (2016).

44. Laussy, F. P., Kavokin, A. V. & Shelykh, I. A. Exciton-Polariton Mediated Superconductivity. *Phys. Rev. Lett.* **104,** 106402 (2010).

45. Malpuech, G. *et al.* Polariton Lasing Due to the Exciton-Electron Scattering in Semiconductor Microcavities. *Phys. status solidi* **190,** 181–186 (2002).

46. Venkateshvaran, D. *et al.* Approaching disorder-free transport in high-mobility conjugated

polymers. *Nature* **515,** 384–388 (2014).

Acknowledgements. This research was financially supported by the European Research Council under the European Union's Seventh Framework Programme (FP/2007-2013)/ERC Grant Agreement No. 306298 (EN-LUMINATE) and under the European Union's Horizon 2020 Framework Programme (FP/2014-2020)/ERC Grant Agreement No. 640012 (ABLASE) and by the Scottish Funding Council (through SUPA). L.T. thanks the EPSRC for support through the CM-DTC (EP/L015110/1). J.Z. thanks the Alfried Krupp von Bohlen und Halbach-Stiftung via the "Alfried Krupp Förderpreis für junge Hochschullehrer" for general support.

Author contribution. A.G. and M.H. performed the experiments, simulations and analysed the data. Y.Z. assisted with interpretation and data analysis. L.T. contributed to the simulations. A.G., M.C.G. and J.Z. jointly wrote the manuscript. M.C.G. and J.Z. conceived and supervised the project. All authors discussed the results and commented on the manuscript.

Competing financial interests. The authors declare no competing financial interests.

Methods

Fabrication of SWCNT-cavity-LEFETs. A top-gate/bottom-contact transistor structure was integrated into a photonic microcavity. The bottom cavity mirror consisted of 2 nm Cr and 30 nm Au, evaporated through a shadow mask onto a low sodium glass substrate (Schott AF32 Eco). Subsequently, the bottom aluminum oxide spacer layer was deposited by atomic layer deposition (Ultratech Savannah S100) at 200 °C using trimethylaluminium as precursor and water as the oxygen source. The thickness of this spacer layer, which defines the cavity detuning, was varied between 130 nm and 310 nm (see Table S1). Photolithography, electron-beam evaporation of 2 nm Cr/ 30 nm Au and lift-off were employed to pattern interdigitated source-drain electrodes with channel lengths of L = 5, 10, 20 and 40 μm and widths of W = 10 mm and 5 mm, resulting in W/L = 2000, 1000, 500 and 125, respectively.

Dispersions of (6,5) SWCNTs in toluene were prepared from CoMoCAT® raw material (773735, Lot #14J017A1, Sigma Aldrich). 70 mg PFO-BPy (poly[(9,9-dioctylfluorenyl-2,7-diyl)-*alt-co*-(6,6'-{2,2'-bipyridine})], American Dye Source, M_W = 34 kg mol^{-1}) were dissolved in 140 mL of toluene before adding 53 mg of CoMoCAT-SWCNTs. Shear force mixing (Silverson L5M-A) was then applied at maximum speed (10,230 rpm) for up to 96 h. The dispersion step was followed by subsequent centrifugation at 60,000 g (Beckman Coulter Avanti JXP centrifuge) for 60 min with an intermediate supernatant extraction and centrifuge tube exchange after 30 min. The final supernatant contained high-purity (6,5) SWCNTs that were further enriched by repeatedly pelleting the dispersions via ultracentrifugation at 284,600 g. The final SWCNT concentration was adjusted by dispersing different amounts of pellets in small volumes of toluene. The dispersions were spin-coated at 1000 rpm on top of the source-drain electrodes. Two different SWCNT layers with a thickness of 33 ± 8 nm and 19 ± 3 nm were investigated here (see Supplementary Fig. 1).

Absorption spectra of SWCNT films were recorded with a Cary 6000i UV/Vis/NIR absorption spectrometer (Varian). Before applying the hybrid gate dielectric, the SWCNT films were annealed at 300 °C in a dry nitrogen atmosphere for 45 min to remove water and residual organic solvent. The hybrid dielectric consisted of two layers: poly(methyl methacrylate) (PMMA) and hafnium oxide (HfO_x). First, 6 mg mL^{-1} of PMMA (Polymer Source, syndiotactic, M_w = 300 kg mol^{-1}) in anhydrous n-butylacetate were spin-coated at 6000 rpm to yield an 11 nm film. After annealing at 80°C, a 61 nm HfO_x layer was added by atomic layer deposition (Ultratech Savannah S100) at 100 °C using tetrakis(dimethylamino)hafnium as a precursor and water as the oxygen source. 60 nm of thermally evaporated silver formed the gate electrode of the transistor and the top mirror of the cavity.

Optoelectronic characterization.

Current-voltage characteristics were recorded with an Agilent 4156C Semiconductor Parameter Analyzer or a Keithley 2612A source meter. Gate dielectric capacitances were measured with an Agilent E4980A Precision LCR Meter. The linear charge carrier mobilities were calculated from the transfer characteristics at a drain voltage $V_d = \pm 0.5$ V assuming the gradual channel approximation for field-effect transistors and using a measured areal capacitance of C = 100-150 nF cm^{-2}. The current density in these devices is calculated from the measured drain current by using the known width of the channel and assuming a 5 nm thick accumulation layer. To estimate the exciton pumping rate, we assumed a 1 µm wide recombination zone, which corresponds to the experimentally observed emission zone width.

A Fourier imaging setup was employed for angle-resolved measurements. For reflectivity measurements, the light of a calibrated tungsten lamp was focused (spot diameter, ~3 µm) onto the transistor channel through a NIR corrected ×100 objective with 0.8 NA (Olympus LMPL100xIR).

The reflectivity of the cavity was then calculated with respect to a spot next to the cavity where only the top gate was present. For PL measurements, SWCNTs were excited by a laser diode (OBIS, Coherent Inc., 640 nm, cw, ~10 mW) while for EL measurements drain and gate voltages were applied. Using the Fourier imaging system, the light reflected/emitted by the LEFET was imaged onto the entrance slit of the spectrometer (Princeton Instruments IsoPlane) and detected by a thermoelectrically cooled 640×512 InGaAs array camera (Princeton Instruments, NIRvana:640ST). Additionally, a long-pass filter (cut-off wavelength, 850 nm) and a linear polarizer were placed in front of the spectrometer. EL spectra of a reference LEFET were recorded with an Acton SpectraPro SP2358 spectrometer (grating 150 lines/mm) and a liquid nitrogen-cooled InGaAs line camera (Princeton Instruments OMA V:1024 1.7). The emission was collected through a near-infrared ×50 objective with 0.65 NA (Olympus LCPLN50XIR).

The PL quantum yield (PLQY) of SWCNT layers was determined with an integrating sphere. The number of emitted photons and absorbed photons were recorded simultaneously and the ratio gave the PLQY.

To determine the external quantum efficiency (EQE) of LEFETs, we measured the total light output with a calibrated InGaAs photodiode (Thorlabs FGA21-CAL, active area 3.1 mm^2) positioned underneath our devices to enable collection of most of the outcoupled light. The EQE, defined as the number of detected photons divided by the number of injected charges, was calculated from the maximum photocurrent I_{diode} of the photodiode (at 0 V bias) during a sweep of the gate voltage for a constant drain current (I_{d}) according to:

$$EQE = \frac{I_{\mathrm{diode}}}{I_{\mathrm{d}}} \cdot \frac{\int \lambda \cdot EL_{\mathrm{norm}}(\lambda)\mathrm{d}\lambda}{\int S(\lambda) \cdot EL_{\mathrm{norm}}(\lambda)\mathrm{d}\lambda} \cdot \frac{e}{hc} \qquad (1)$$

with $S(\lambda)$ as the wavelength-depended sensitivity of the photodiode weighted by the normalized $EL_{\mathrm{norm}}(\lambda)$ spectrum of the respective LEFET.

Coupled oscillator model. The observed polariton branches were fitted with the coupled oscillator model. By introducing a coupling potential V_{A} the new eigenstates of the exciton-photon system are given by

$$E_{\mathrm{UP/LP}} = {}^{1}/_{2} \cdot (E_{\mathrm{X}} - i\hbar\Gamma_{\mathrm{X}} + E_{\mathrm{C}} - i\hbar\Gamma_{\mathrm{C}}) \pm \sqrt{{V_{\mathrm{A}}}^{2} + {}^{1}/_{4} \cdot (E_{\mathrm{X}} - i\hbar\Gamma_{\mathrm{X}} - (E_{\mathrm{C}} - i\hbar\Gamma_{\mathrm{C}}))^{2}}\,, \qquad (2)$$

where E_{X} is the exciton energy with a homogenously broadened HWHM $\hbar\Gamma_{\mathrm{X}}$ and E_{C} the cavity mode with a HWHM $\hbar\Gamma_{\mathrm{C}}$.[47] The energy dispersion of the cavity is described by

$$E_{\mathrm{C}}(\theta) = E_0\,(1 - (\sin(\theta)/n_{\mathrm{eff}})^2)^{-1/2} \qquad (3)$$

for a cavity tuned to $E_0 = E_{\mathrm{X}} + \Delta$ with Δ being the cavity detuning. The effective refractive index n_{eff} was determined from a reference cavity (1.96 for TE and 2.53 for TM polarization). The coupling potential V_{A} is related to the Rabi splitting by $V_{\mathrm{A}} = 0.5 \cdot \sqrt{\hbar\Omega^2 + (\hbar\Gamma_{\mathrm{C}} - \hbar\Gamma_{\mathrm{X}})^2}$ at $E_{\mathrm{C}} = E_{\mathrm{X}}$. In this picture strong coupling and hybridization occur when $\hbar\Omega > \hbar\Gamma_{\mathrm{X}} + \hbar\Gamma_{\mathrm{CM}}$.[48] The photonic (excitonic) fractions $\alpha(\beta)$ of the polaritonic states are calculated by their projection onto the uncoupled states.

47. Bajoni, D. Polariton lasers. Hybrid light–matter lasers without inversion. *J. Phys. D. Appl. Phys.* **45,** 409501 (2012).

48. Liu, X. *et al.* Strong light–matter coupling in two-dimensional atomic crystals. *Nat. Photonics* **9,** 30–34 (2014).

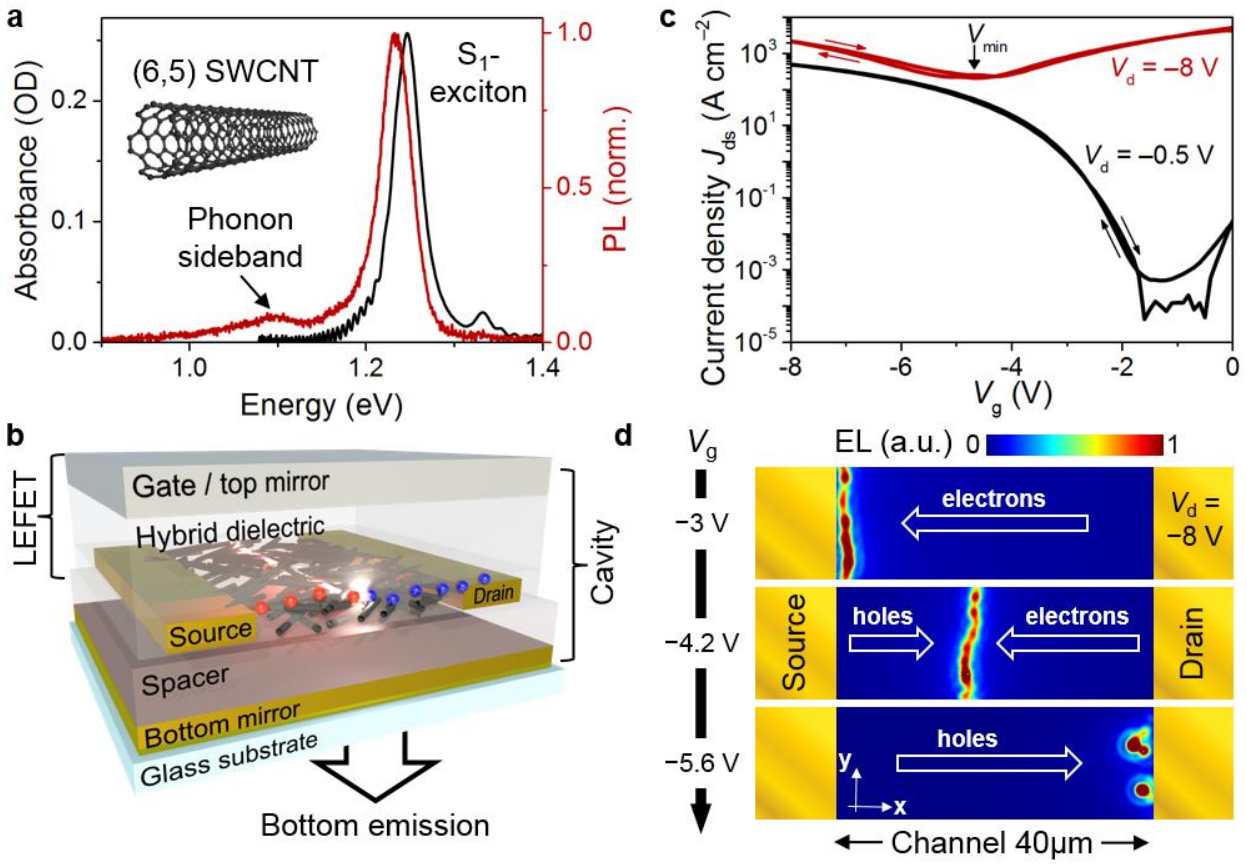

Figure 1 | Single-walled carbon nanotube-based light-emitting field-effect transistors. a, Absorbance and PL spectra of (6,5) SWCNTs embedded in a polymer (PFO-BPy) matrix. **b**, Schematic geometry of a bottom-contact/top-gate LEFET (top stack). By extending the structure with a bottom mirror an optical microcavity is formed between the top gate and the bottom mirror. **c**, Transfer characteristics of the cavity-embedded transistor for low and high source-drain bias (V_d). Electroluminescence is observed in the ambipolar regime at higher drain bias (V_d = –8 V), around the gate voltage V_{min}. **d**, Real-space images of the near-infrared electroluminescence for different gate voltages (see also supplementary video).

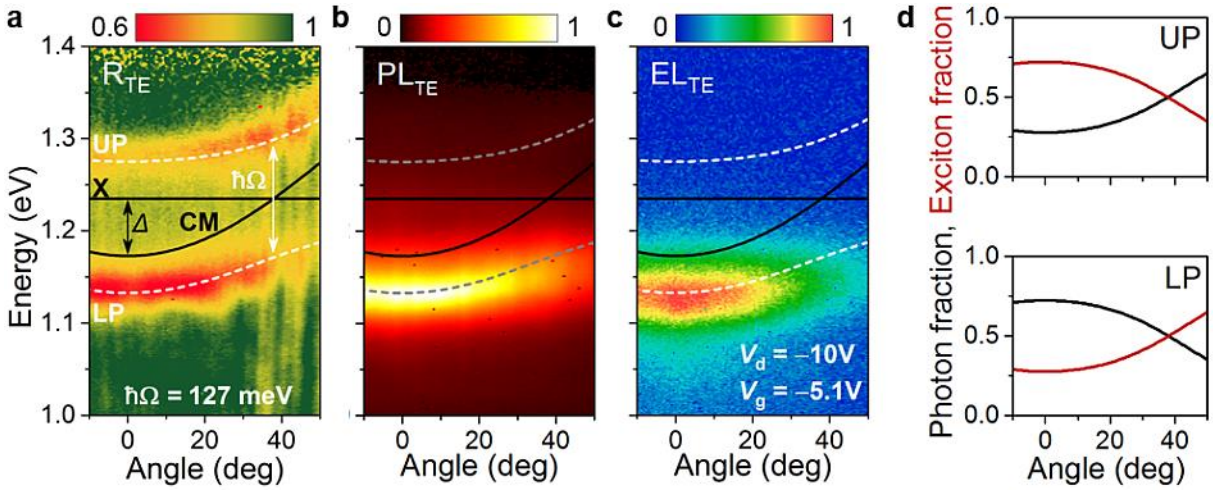

Figure 2 | Exciton-polaritons in light-emitting field-effect transistors. a, Angular reflectivity of the channel area in an LEFET-cavity with a dense (6,5) SWCNT layer (thickness, 33 nm). The dispersionless black solid line indicates the exciton (X) and the parabolic black line the cavity mode (CM). Strong exciton-photon coupling leads to the formation of a UP and LP mode (white dashed lines, fitted with the coupled oscillator model). **b**, Angle and spectrally resolved emission under optical excitation. **c**, Angle and spectrally resolved electroluminescence. **d**, Angle-dependent photon and exciton fraction of the UP (top) and LP (bottom) as calculated by the coupled oscillator model. All data shown for TE polarization (see Supplementary Fig. S4 for TM).

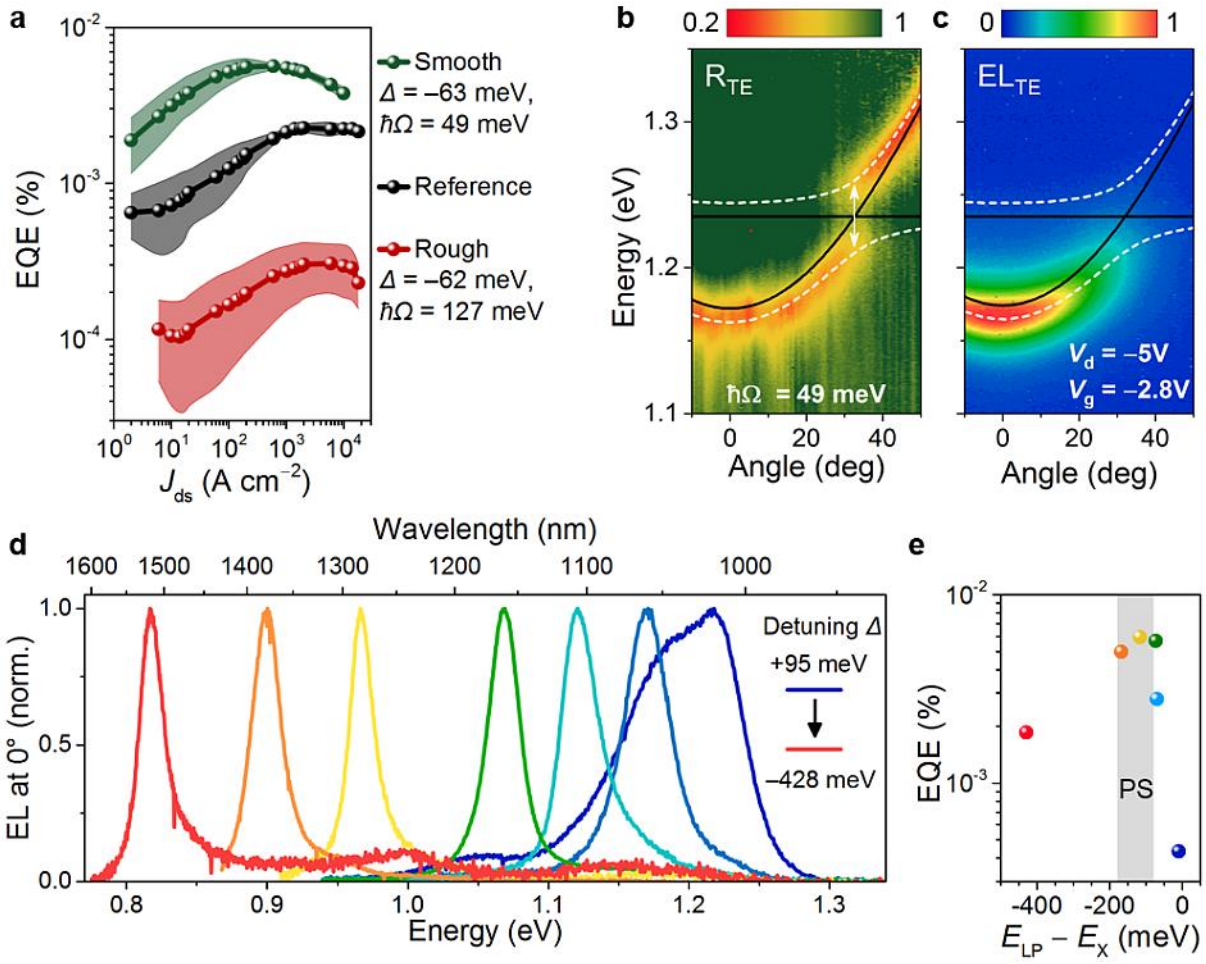

Figure 3 | Tunable electrically pumped exciton-polaritons. a, External quantum efficiency (EQE) for LEFETs in the strong coupling regime with rough (red) and improved, smooth (green) SWCNT layer. The black data points represent a reference LEFET without cavity. The shaded region indicates experimental uncertainties. **b**, Angular reflectivity of an LEFET transistor with a smooth, 19 nm layer of SWCNTs. **c**, Angle-resolved electroluminescence from the same transistor. **d**, EL emission spectra normal to the sample surface for SWCNT-based polariton-LEFETs with different detuning values (see Supplementary Fig. S7). **e**, EQE versus energy difference of the LP and exciton for devices shown in d. The grey shaded area represents the overlap of the LP with the phonon sideband of the (6,5) SWCNTs.

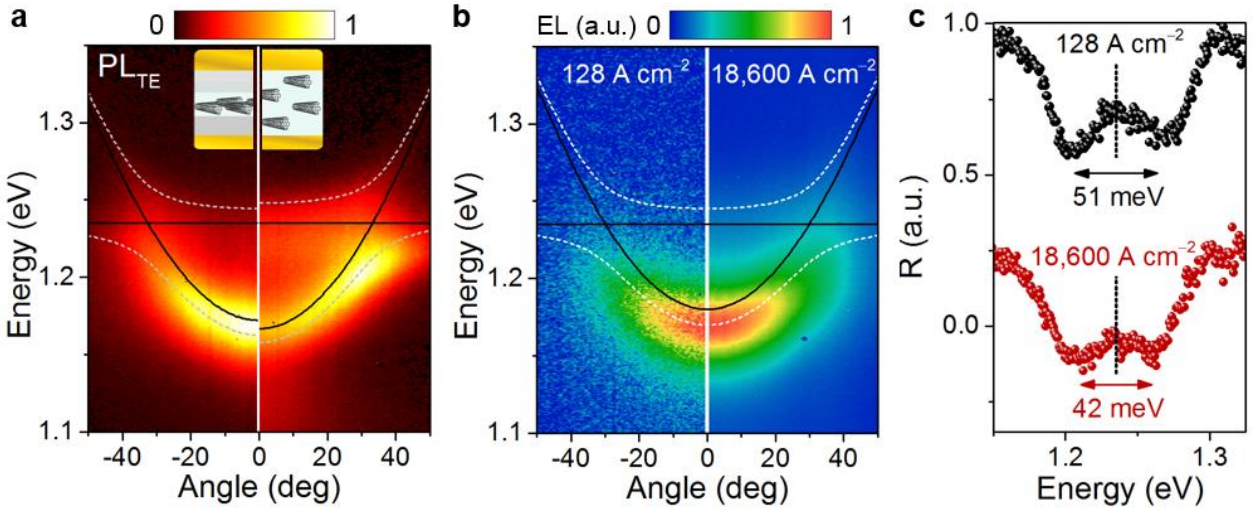

Figure 4 | Enhanced relaxation and polaritons at high current densities. a, Angular PL of the LP for the channel area in an LEFET-cavity (left) and in an optical microcavity as in Ref. [18] (right). The thickness (19 nm vs. 250 nm) and density (39 wt% vs. 0.5 wt%) of the two SWCNTs layers lead to similar polariton modes but very different relaxation behaviour. **b**, Angular electroluminescence (EL) at low (left) and high (right) current densities for the LEFET in Figure 3b. **c**, Reflectivity at an angle of 29° (exciton and photon are resonant) revealing 17 % smaller Rabi splitting at high current densities but still clear strong coupling. The dashed line represents the exciton energy.

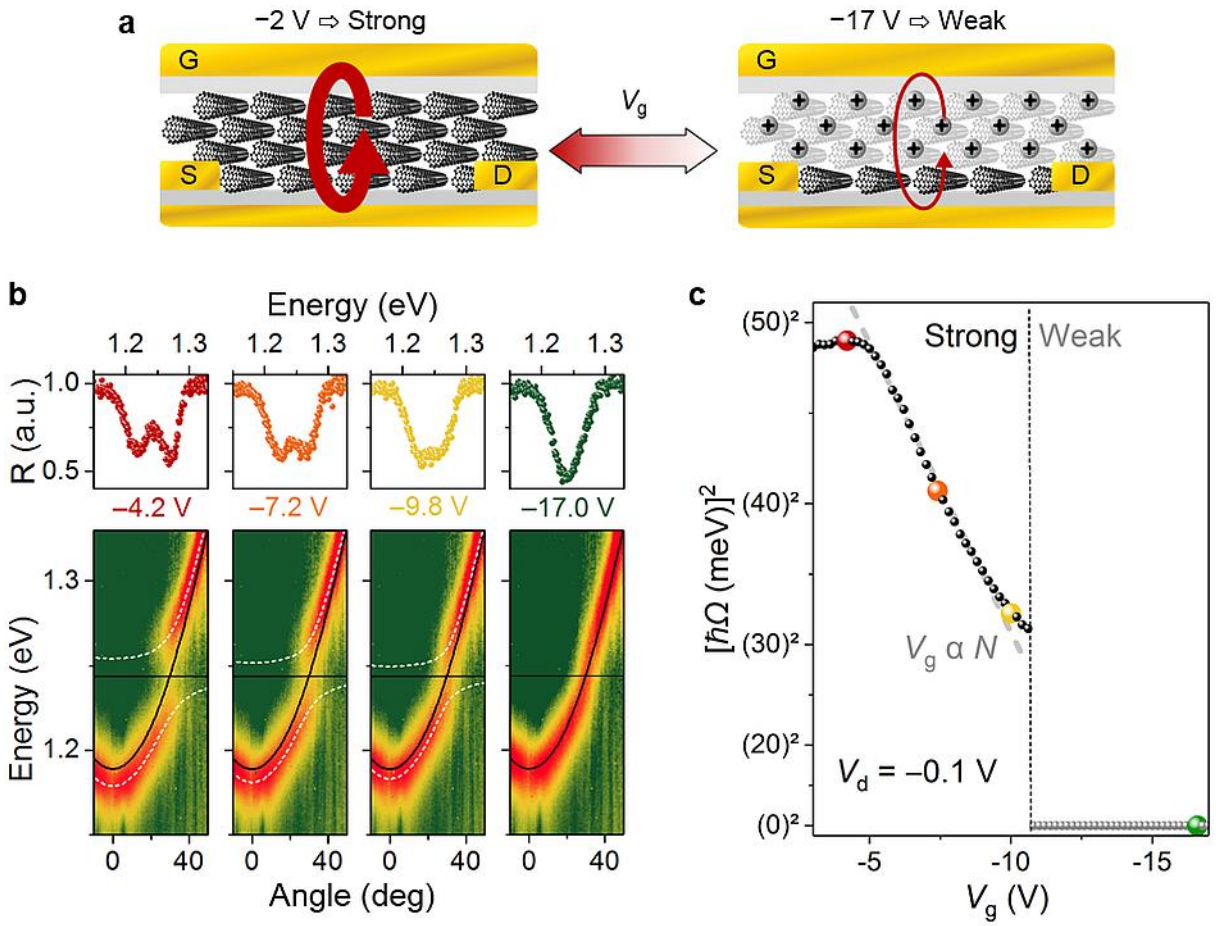

Figure 5 | Reversible tuning between strong and weak coupling in LEFETs. a, Schematic illustration of tuning between strong coupling in uncharged SWCNTs at low gate voltages and weak coupling due to hole accumulation in the nanotubes and bleaching at large negative gate voltages. **b**, Representative reflectivity under 29° angle of incidence ($E_X = E_C$, top) and angular reflectivity spectra (bottom) at four different gate voltages. **c**, Square of Rabi splitting $\hbar\Omega$, determined from angular reflectivity measurements, versus applied gate voltage in unipolar regime (black symbols). The accumulated charges (holes) and thus bleaching of S_1 absorption increase linearly with gate voltage V_g (dashed line). Coloured circles correspond to data in **b**.